Journal of Materials Chemistry C

A multifunctional hole-transporter for high-performance TADF OLEDs and clarification of factors governing the transport property by multiscale simulation

Journal:	*Journal of Materials Chemistry C*
Manuscript ID	TC-ART-02-2022-000716.R1
Article Type:	Paper
Date Submitted by the Author:	13-Apr-2022
Complete List of Authors:	Nagamura, Natsuo; Yamagata univ., Organic Device Engineering Sasabe, Hisahiro; Yamagata univ., Organic Device Engineering Sato, Hiroki; Kyoto University Kamata, Takahiro; Yamagata University, Department of Organic Device Engineering Ito, Nozomi; Yamagata univ., Organic Device Engineering Araki, Suguru; Yamagata univ., Organic Device Engineering Abe, Shoki; Yamagata univ., Organic Device Engineering Sukegawa, Yoshihito; Yamagata univ., Organic Device Engineering Yokoyama, Daisuke; Yamagata University, Department of Organic Materials Science Kaji, Hironori; Kyoto University, Institute for Chemical Research Kido, Junji; Yamagata Daigaku

SCHOLARONE™
Manuscripts

A multifunctional hole-transporter for high-performance TADF OLEDs and clarification of factors governing the transport property by multiscale simulation

Natsuo Nagamura[1], Hisahiro Sasabe[1,2,3], Hiroki Sato[4], Takahiro Kamata[1], Nozomi Ito[1], Suguru Araki[1], Shoki Abe[1], Yoshihito Sukegawa[1], Daisuke Yokoyama[1,2], Hironori Kaji*[4], Junji Kido*[1,2,3]*

[1]Department of Organic Materials Science, Yamagata University, 4-3-16 Jonan, Yonezawa, Yamagata 992-8510, Japan, [2]Research Center of Organic Electronics (ROEL), Yamagata University, 4-3-16 Jonan, Yonezawa, Yamagata 992-8510, Japan, [3]Frontier Center for Organic Materials (FROM), Yamagata University, 4-3-16 Jonan, Yonezawa, Yamagata 992-8510, Japan, [4]Institute for Chemical Research, Kyoto University Uji, Kyoto 611-0011, Japan
E-mail: h-sasabe@yz.yamagata-u.ac.jp; kaji@scl.kyoto-u.ac.jp; kid@yz.yamagata-u.ac.jp

Keywords: (thermally activated delayed fluorescence, long lifetime, hole-transporter, hexaphenylbenzene derivative, multiscale simulation)

Abstract: To-this-date, a limited number of reports has been published on thermally activated delayed fluorescent (TADF) organic light-emitting devices (OLEDs) that simultaneously achieved high efficiencies and long operational lifetimes. The development of tailored-hole transporters is an effective solution because extensively used conventional hole-transport materials (HTMs), such as **NPD** or **TAPC**, are unsuitable for simultaneous realizations of high-efficiency and long-lifetime in TADF OLEDs. In this study, we developed a new four-dibenzofuran (DBF) end-capped hexaphenylbenzene (HPB)-based HTM, referred to as **T4DBFHPB**. Using this as the HTM, we simultaneously achieved high external quantum efficiency (η_{ext} = 22.0 %), long operational lifetime (LT_{50} = 28000 h), and low-drive voltage (3.83 V) at 1000 cd m^{-2} in green TADF OLEDs. Our research reveals the importance of multifunctional HTM with (i) high triplet energy (E_T), (ii) high glass transition temperature (T_g), and (iii) high bond dissociation energy (BDE) of the C-N bonds in the anion state. Moreover, we conducted multiscale simulations to improve the hole-mobility (μ_h). Consequently, the simulation suggested that permanent-dipole-induced site energy and reorganization energy are critical factors for improving μ_h among HPB derivatives.

1. Introduction

Organic light-emitting devices (OLEDs) based on thermally activated delayed fluorescent (TADF) emitters are potential candidates for future low-power consumption displays.[1] TADF OLEDs, the so-called third-generation OLEDs, can achieve 100% electron-to-phonon conversion by using all the singlet and triplet molecular excitons, like second-generation phosphorescent emitters[2] without using rare metal elements.

For phosphorescent and TADF OLEDs, neighboring materials, for example host materials and carrier transport materials, such as hole-transport and electron-transport materials (HTMs and ETMs), are required to have higher triplet energies (E_T) than that of the emitter molecule. This is because triplet excitons, which account for 75% of all excitons contributing to emission, should be confined to the emitting layer to boost the efficiency.[2, 3] In addition, a high-chemical stability is required for long operational lifetimes.[2, 3, 4] As for TADF, the ionization potential (I_p) of the HTMs should be sufficiently deep to suppress the potential exciplex formation with TADF emitters. A narrow gap exciplex formation causes exciton quenching and deteriorates the efficiency. [5, 6]

To-this-date, only a limited number of reports has been published on green TADF OLEDs that simultaneously achieve high efficiencies and long operational lifetimes. An

early example of a green TADF OLED is **4CzIPN**-based TADF reported by Nakanotani and Adachi.[7, 6a] The device showed an external quantum efficiency (η_{ext}) of 14% and an operation lifetime at 50% of the initial luminance (LT_{50}) of 2800 h at 1000 cd m^{-2}. This research suggests that the recombination zone localized at the interfaces between the emission layer (EML) and the neighboring layers (ETM or HTM) deteriorates the neighboring materials and lead to the low efficiency and the short operational lifetime. Therefore, improvements in the carrier balance and chemical stability of the ETM and HTM are required. In a subsequent work, they also noted that they realized an η_{ext} of 19.2% and an LT_{50} of 10934 h at 1000 cd m^{-2} in **4CzIPN**-based green TADF OLED with the use of tailored triphenyltriazine-based n-type hosts.[6b] Recently, Sasabe and Kido developed a series of hexaphenylbenzene (HPB)-based dibenzofuran (DBF) or dibenzothiophene (DBT)-end-capped HTMs and applied it to green TADF OLEDs.[8] By using **4DBFHPB** depicted in **Figure 1** as the HTM, they achieved an η_{ext} of 19.2%, drive voltage of 4.07 V at 1000 cd m^{-2}, and LT_{50} of 24000 h at 1000 cd m^{-2}. This work suggests that (i) introduction of DBF or DBT-end-capping groups deepens the I_p and improves the bond dissociation energy (BDE) of the C-N bonds in the anion state compared with the phenyl-end-capping counterpart, and (ii) the deep I_p, high E_T, and the larger BDEs in anion states are three key factors for simultaneously improving the

efficiency and operational lifetime in TADF OLEDs.

To further improve the OLED lifetime, in this study, **T4DBFHPB** is fully end-capped by four DBFs without phenyl-end-capping groups, and has larger BDEs compared with phenyl-end-capping counterpart maintaining a high E_T value of 2.8 eV. Using **T4DBFHPB** as the HTM, we simultaneously achieved high η_{ext} of 22.0%, LT_{50} of 28000 h, and low-drive voltage of 3.83 V at 1000 cd m^{-2} in green TADF OLEDs. Further, to clarify the governing factors of hole-transport property, we conducted the multiscale simulation.[9,10] Consequently, the multiscale simulation analyses suggested that permanent-dipole-induced site energy and reorganization energy are critical factors for improving μ_h of **T4DBFHPB**.

2. Results and discussion

2.1. Molecular design and density functional theory calculation

Hole-transporters based on the HPB core have a high E_T due to the twisted molecular structure (**Figure 1**). Because the magnitude of the intermolecular interaction is inversely proportional to the intermolecular distance, the large exclusive volumes of the HPB derivatives could also reduce the exciton quenching derived from the narrow-gap exciplex formation.[8] Moreover, their large molecular weights are expected to enhance

the thermal stability. Compared with the simplest structure of **TATT**[8a] with four phenyl-end-capping groups, DBF-end-capped **4DBFHPB** improved the two of four poor BDEs of the C-N bonds, which led to LT_{50} values >2 times higher than those of the **TATT**. To further improve the OLED lifetime, **T4DBFHPB** is fully end-capped by the four DBF groups. Before synthesizing this new compound, density functional theory (DFT) calculations were conducted. The optimized structure of the neutral ground state was calculated at the RB3LYP 6-31G(d) theory level. The single-point energies were calculated at the RB3LYP 6-311+G(d,p) level of theory. Singlet (E_S) and triplet energies (E_T) were calculated with the use of time-dependent DFT (TD-DFT) (**Figure 2**). The calculated E_T of **T4DBFHPB** (2.83 eV) was slightly higher than that of **4DBFHPB** (2.79 eV). We also conducted DFT calculations of the BDE of the anionic state based on the URB3LYP 6-31G(d) theory level (**Figure S1**) [11]. The calculated BDE of the C-N bond of **T4DBFHPB** was 1.72 eV, which was significantly stronger than that of **TATT** (1.52 eV). In addition, the high molecular weight of **T4DBFHPB** (MW = 1229) is expected to improve the thermal stability.

2.2. Synthesis

The synthetic route to **T4DBFHPB** is shown in **Scheme S1**. A Buchwald-Hartwig

amination reaction of a dibrominated HPB and the corresponding dibenzofuran-modified amine produced the target compound with a yield of 78%. The target compound was identified by ^{1}H nuclear magnetic resonance (^{1}H-NMR), ^{13}C-NMR (**Figure S2, S3**), mass spectrometry (MS), and elemental analyses. The compounds were successfully purified by train sublimation despite the large molecular weight (MW = 1229), and the purities were confirmed to be greater than 99.5% by high-performance liquid chromatography (HPLC).

2.3. Thermal and physical properties

The thermal properties of the materials were estimated using differential scanning calorimetry (DSC) and thermogravimetric analysis (TGA). **T4DBFHPB** showed a very high-glass transition temperature (T_g) of 171 °C, a high-melting point (T_m) of 364 °C, and a high-decomposition temperature (T_{d5}) of 494 °C. The T_g was apparently higher than that of **4DBFHPB** (135 °C)[8c] and **NPD** (95 °C)[12] presumably due to the large molecular weight. Therefore, the thermal stability and the enhanced stability of the device were expected to be improved in the thin solid film form used in OLEDs. The optical properties of the solid thin films made by the vacuum evaporation method were then evaluated. I_P and the energy gap (E_g) of **T4DBFHPB** were determined using

photoelectron yield spectroscopy (PYS)[13] and ultraviolet-visible (UV-vis) absorption spectroscopy, respectively (**Figure S4**). **T4DBFHPB** exhibited deep I_p of −5.6 eV, and wide E_g of 3.3 eV. The electron affinities (E_a) were estimated to be $E_a = I_p + E_g = -2.3$ eV. As expected from the DFT calculations, the material also exhibited a high E_T value of 2.8 eV from the onset of the phosphorescence spectra at 5 K (**Figure S5**). Compared with **4DBFHPB** with two DBF groups, **T4DBFHPB** with four DBF groups showed significantly greater T_g of 171 ˚C, 0.2 eV shallower I_p, and slightly higher E_T of 2.8 eV. All the thermal and physical properties are summarized in **Table 1**. Then, we also examined the molecular orientation with the use of variable-angle spectroscopic ellipsometry (VASE)[14] (**Figure S6**). The analyzed order parameter S_{VASE} was −0.16, which was slightly smaller than that of **4DBFHPB** ($S_{VASE} = -0.13$) most likely due to the larger π-plane of DBF groups than that of phenyl groups. Thus, **T4DBFHPB** was slightly more horizontally oriented than **4DBFHPB**. Note that $S_{VASE} = -0.5$ means perfectly horizontally oriented, while $S_{VASE} = 0$ and 1.0 mean randomly and perfectly vertically oriented, respectively.

2.4. TOF measurements

We measured the TOF values to evaluate the hole-mobility. The device structure was

used in the measurements: [ITO (100 nm)/**T4DBFHPB** (5.27 μm)/Al (20 nm)]. The measured hole-mobility was 6.0×10^{-4} cm^2 V^{-1} s^{-1} in an electric field of 5.6×10^5 V cm^{-1}. The corresponding hole-mobility of **4DBFHPB** was reported to be 1.5×10^{-3} cm^2 V^{-1} s^{-1}, which is greater than that of **T4DBFHPB**.

The transport parameters were also analyzed by using the Gaussian disorder model (**Table 2**). [15] For this purpose, the mobility was measured at various temperatures (**Figure S7**). **Figure 3** shows the field dependence of the mobility of **4DBFHPB** and **T4DBFHPB** at a temperature of 298 K. The Poole-Frenkel dependence of $\mu \propto e^{\gamma\sqrt{F}}$ can be observed in both materials. The mobility of **T4DBFHPB** is smaller than that of **4DBFHPB** in all regions of the applied field. The hypothetical mobility μ_0 in the disorder-free system was larger in **4DBFHPB**. The energetic disorders (σ) of **4DBFHPB** and **T4DBFHPB** are 96 meV and 90 meV, respectively. The positional disorders (Σ) were **4DBFHPB** (1.40) < **T4DBFHPB** (1.80). As such, **T4DBFHPB** exhibited 1/2.5 smaller μ_h compared with that of **4DBFHPB**, slightly more horizontally oriented (S_{VASE} = −0.16), smaller energetic disorder σ ($\Delta\sigma$ = 6 meV), and larger positional disorder Σ ($\Delta\Sigma$ = 0.40). Among these factors, smaller S_{VASE} and σ values could contribute to enhance the μ_h. Therefore, positional disorder Σ seems to be an important factor to reduce the μ_h value in **T4DBFHPB**. However, it is difficult to

extract the governing factors to enhance μ_h in the molecular level by using the Gaussian disorder model.

2.5. Multiscale simulation

To clarify the governing factors in the hole-mobilities between **4DBFHPB** and **T4DBFHPB**, we conducted a multiscale simulation developed by Kaji and co-workers.[10] The simulation consisted of the following parts:

1) The molecular dynamics (MD) calculation to generate the amorphous morphology,

2) The quantum mechanics calculation to evaluate the charge-transfer rate constants, and 3) The kinetic Monte Carlo (kMC) simulation to simulate the TOF experiments.

The site energy statistics, the density of states (DOS), are summarized in **Figure 4**. As the intermolecular site energy, the electrostatic interaction with bare neighboring neutral molecules and the polarization effect were taken into account (See SI). HOMO−p (p = 0, 1, 2, 3) were considered in the mobility calculation, where HOMO−0 is HOMO. In both **4DBFHPB** and **T4DBFHPB**, average energy difference between HOMO and HOMO−1 is within 50 meV. On the other hand, the energy gaps between HOMO−1 and HOMO−2 are larger than the DOS widths (about 100 meV), thus prevent the hopping event to the deeper orbitals in both of the HTMs (**Table S1)**. According to a detailed

analysis (**Table S2)**, the disorder of the site energy of **T4DBFHPB** is greater than that of **4DBFHPB**. This difference is disadvantage for the mobility of **T4DBFHPB**. It was also clarified that the difference between the energetic disorders of **4DBFHPB** and **T4DBFHPB** mainly comes from the intermolecular site energy. For more detail, randomly oriented local permanent dipole moments induced by the oxygen atoms of the dibenzofuran-substructures contribute to the difference of the intermolecular site energy. However, due to some cancelations, the total dipole moments of symmetric **T4DBFHPB** seems smaller than that of asymmetric **4DBFHPB** on average. (**Figure S8**) Therefore, we emphasize the importance of the local permanent dipole moments in dibenzofuran-end-capped HTMs.

Electronic couplings of the molecular pairs within intermolecular distance (distance of the each arithmetic mean of the all atoms coordinates of each molecule) of 3.0 nm in **4DBFHPB** and 3.5 nm in **T4DBFHPB** were calculated. The cut off distances were confirmed to be appropriate from the ratio of the connected pairs which any of H_{ij}^{pq} is > 0.1 meV (In our simulation, the hoppings hardly occur among the pairs whose H_{ij}^{pq} is below this threshold value) to all of the pairs. (**Figure S9**) Where, H_{ij}^{pq} indicates the electronic couplings between the HOMO−*p* of the *i*th molecule and the HOMO−*q* of the *j*th molecule. Distributions of H_{ij}^{pq} are shown in **Figure S10**. The distributions were

investigated in the range of H_{ij}^{pq} from 1 meV to 100 meV, which mainly contribute to the mobility. Because the site energy restricts the hopping to HOMO–p $(p = 0, 1)$, H_{ij}^{00}, H_{ij}^{01} and H_{ij}^{11} are the dominant factors. Thus, electronic couplings are seems to be slightly more advantageous in **T4DBFHPB** than **4DBFHPB**. Scatter plots of H_{ij}^{pq} vs. intermolecular distance are also shown in **Figure S11**. From this figure, the electronic couplings of **T4DBFHPB** are proved to distribute in further intermolecular distance than that of **4DBFHPB**. This means that larger π-plane of the dibenzofuran units in **T4DBFHPB** overlaps more effectively than smaller π-plane of the phenyl units in **4DBFHPB**. The electronic couplings of the both HTMs have potential to be improved when the substituted dibenzofurans are suitably positioned.

The reorganization energy λ was calculated from the optimized geometry of one molecule. The λ values of **4DBFHPB** and **T4DBFHPB** were 0.13 eV and 0.18 eV, respectively. The differences between the optimized geometries of the neutral and cation states are shown in **Figure S12**. The root-mean-square deviations (RMSD) of the atomic positions were 0.150 Å and 1.16 Å for **4DBFHPB** and **T4DBFHPB**, respectively. These structural relaxations mainly come from the variations of the conformers induced by the asymmetrically substituted dibenzofuran units, thus the reduced flexibility of the chemical structure around the nitrogen atoms is one of the

most possible ways to reduce the reorganization energy.

The charge-transfer rate constants k_{ij}^{pq} were calculated from the formula based on Marcus theory [16]:

$$k_{ij}^{pq} = \frac{\left|H_{ij}^{pq}\right|^2}{\hbar}\left(\frac{\pi}{\lambda\, k_B T}\right)^{1/2} \exp\left[-\frac{\left(\lambda + \Delta E_{ij}^{pq} - q\boldsymbol{F}\cdot\boldsymbol{r}_{ij}\right)^2}{4\lambda\, k_B T}\right]. \qquad (1)$$

Where $\Delta E_{ij}^{pq} = E_j^{\mathrm{H}-q} - E_i^{\mathrm{H}-p}$, $\boldsymbol{r}_{ij}$ is the vector from the *i*th to the *j*th molecules, and $\boldsymbol{F}$ ($|\boldsymbol{F}| = F$) is the externally applied electric field.

Then, the kMC simulation based on the calculated hopping rate constants was conducted. The field dependence of the evaluated mobility is shown in **Figure 5**. The results well reproduced the mobilities measured by the TOF.

In order to feedback the results of the simulation to the molecular design, we estimated the contributions to the mobility from the following four factors: a) electronic coupling b) intramolecular site energy, c) intermolecular site energy, and d) reorganization energy. The uniqueness of the molecular structure is reflected on the mobility through these factors which appear in the equation (1). But the contributions of the factors cannot be clear by using factors obtained by calculation, so we conducted the kMC simulations with each factor varied and estimated the contributions using analysis of variance (see SI, **Figure S13-18**). The governing factors of the hole-mobility between **4DBFHPB** and **T4DBFHPB** are shown in **Table 3** (more detail in **Figure S19**). As a

result the intermolecular site energy and the reorganization energy are clearly proved to be factors for improving μ_h. Despite the contribution of the intermolecular site energy decrease according to the increase of the applied field, the contribution is always largest. In this way, our analysis clarifies the contributions which are ambiguous until the simple simulation is done. This determines the priority of the possible improvements in the molecular design before synthesis and will realize more rapid and efficient development of HTMs.

As such, there is much room for improvement of the hole-mobility of dibezofuran-end-capped HTMs to reduce the loss from the intermolecular site energy, which is proved to be the dominant factor. A more symmetric structure such that can cancel local permanent dipole moments is preferable to reduce loss from the intermolecular site energy.

2.6. TADF OLED performances

We fabricated a green TADF OLED device with the structure of [ITO (100 nm)/triphenylamine-containing polymer: **PPBI** (20 nm)[17]/**NPD** (10 nm)/**T4DBFHPB** (10 nm)/**mCBP**[18]: 20 wt% **4CzIPN** (30 nm)/**DBT-TRZ**[19] (10 nm)/**DPB**[20]: 20 wt% **Liq** (40 nm)/**Libpp**[21] (1 nm)/Al]. In this device, double HTL **NPD** and

T4DBFHPB were equipped to realize stepwise hole-injection.[22] We used **DBT-TRZ** as the hole-blocking layer and **Liq**-doped **DPB** as the ETL to obtain a long operational stability. All the device performances are summarized in **Table 4**. Compared with **4DBFHPB**-based device, **T4DBFHPB**-based device exhibited superior OLED performances (**Figure 6**). **T4DBFHPB**-device yielded a high $\eta_{ext,1000}$ of 22.0% at a brightness of 1000 cd m^{-2}, and low turn-on voltage of 2.41 V. While, **4DBFHPB**-based device showed slightly lower $\eta_{ext,1000}$ of 19.2% at a brightness of 1000 cd m^{-2}, and higher turn-on voltage of 2.45 V. Then, we performed the stability test at a constant current density (**Figure 6c**). The operational lifetime at 50% of the initial luminance (LT_{50}) at a constant current density of 10 mA cm^{-2} was 506 h for **T4DBFHPB**, while the corresponding LT_{50} for **4DBFHPB** was shorter of 497 h. Finally, we carried out an acceleration test at constant current densities of 20 and 30 mA cm^{-2} (**Figure 6d**). The operational lifetime at an initial luminance of 1000 cd m^{-2} was extrapolated from the formula $L_0^n \times LT\ (L_0) = const.$[23] As a result, **T4DBFHPB**-based device achieved LT_{50} = 28,000 h, while **4DBFHPB**-based device realized shorter LT_{50} = 24,000 h. Note that these devices were sealed at N_2 atmosphere and were not exposed to the air after the spin coating of the polymer buffer layer.

The values of EQE and LT_{50} at 1000 cd/m^2 are improved up to 110% and 120% by

using **T4DBFHPB**. Thus, the following four factors are critically important to improve the stability of **4CzIPN**-based TADF OLEDs: 1) High glass temperature (T_g): The large molecular weight of the **T4DBFHPB** increases the T_g value. 2) Large BDE toward anion state: All of the weak phenyl-end-capping groups are replaced to DBF-end-capping groups leading to greater BDEs. 3) Reduced exciplex formation: The bulky HPB core can prevent the potential exciplex formation. 4) I_P: The well-matched I_P of **T4DBFHPB** to control the hole-injection from the ITO to EML.

In this OLED architecture, hole-injection property is more important than the mobility, the shallower I_p of **T4DBFHPB** significantly increased the hole current density and carrier balance factor leading to the higher EQE. This is because the DOS overlapping with **NPD** is superior for **T4DBFHPB** compared with **4DBFHPB**.[22] However, it should be noted that the shallower I_p increases the potential exciplex formation with TADF emitters and this can lead to the lower EQE depending on the device architecture. **T4DBFHPB**-based device showed the higher EQE and higher current density compared with **4DBFHPB**. Thus, the emission zone is located not at the HTL/EML interface, but at the center of EML to realize higher EQE. This can explain how the shallower I_p of **T4DBFHPB** could improve the EQE. **Table S3** shows the effects of DBF-end-capping groups toward the OLED performances. Compared with other HTM with four

DBF-end-capping groups, the following three merits can be found to use HPB-core skeleton (See also **Table S4**, **S5**, **Figure S20, S21** and **S22**): (i) The mobility of the **T4DBFHPB** is higher than the other HTMs most likely due to the rigid core skeleton to reduce the number of conformers. (ii) The corresponding **T4DBFHPB**-based device achieved the longest lifetimes and the reduced driving voltages maintaining high EQE of over 20% at 1000 cd/m^2. (iii) The highest T_g enhances the thermal stability.

Finally, compared with the state-of-the-art green TADF OLEDs, T4DBFHPB-based device exhibited the best performances with longest lifetimes (**Table 5**).

3. Conclusions

In this study, we successfully developed a novel HTM named **T4DBFHPB** end-capped with four DBF groups for efficient and long-term stability TADF OLEDs. **T4DBFHPB** showed multifunctions such as a higher T_g of 171 ˚C, a greater anionic BDE of 1.72 eV, a higher E_T of 2.8 eV, enhanced μ_h of 6.0×10^{-4} m^2 V^{-1} s^{-1}, and superior OLED performances including the long-term stability compared with the four phenyl groups end-capped **TATT**. Further, compared with **4DBFHPB** end-capped with two DBF groups, **T4DBFHPB** achieved higher efficiency and longer lifetime in green TADF OLEDs maintaining a high T_g, anionic BDE, and E_T with slightly reduced μ_h.

This μ_h value is still smaller than that of **4DBFHPB** (1.5×10^{-3} V cm^{-2} s^{-1}) and **TAPC** (10^{-2} V cm^{-2} s^{-1})[12b], so there is much room for improvement. Beyond the conventional model such as Gaussian disorder model, mobility was investigated with the multiscale simulation to clarify the governing factors in the μ_h. The simulation results reproduced the experimental mobility well. The quantitative analysis using analysis of variance showed that the intermolecular site energy and the reorganization energy are the critical factors for improving μ_h of **T4DBFHPB**. The contribution rates are ambiguous until the quantitative analysis is done. Then, for example, a more symmetric molecular structure that can cancel the local permanent dipole moments will reduce loss from the intermolecular site energy and effectively improve the mobility of dibezofuran-end-capped HTMs. In this way, the parameter free simulation and the quantitative analysis as we have done here provides more reasonable molecular design than the model-dependent conventional analysis.

Supporting Information

Supporting Information is available online.

Acknowledgements

We gratefully acknowledge the partial financial support from the Center of Innovation (COI) Program of the Japan Science and Technology Agency (JST). HS acknowledges financial support in part by JSPS KAKENHI (17H03131, 20H02807) from the JSPS. HK acknowledges financial support in part by JSPS KAKENHI JP20H05840 (Grant-in-Aid for Transformative Research Areas, “Dynamic Exciton”). Computation time for multiscale simulations was provided by the Super Computer System, Institute for Chemical Research, Kyoto University. JK, HS, and HK acknowledges financial support in part by the Collaborative Research Program of Institute for Chemical Research, Kyoto University (grant #2020-103).

References

[1] (a) C. Adachi, *Jpn. J. Appl. Phys.*, **2014**, 53, 060101; (b) Z. Yang, Z. Mao, Z. Xie, Y. Zhang, S. Liu, J. Zhao, J. Xu, Z. Chi and M. P. Aldred, *Chem. Soc. Rev.*, **2017**, 46, 915; (c) Y. Im, M. Kim, Y. J. Cho, J. A. Seo, K. S. Yook and J. Y. Lee, *Chem. Mater.*, **2017**, 29, 1946; (d) M. Y. Wong and E. Z. Colman, *Adv. Mater.*, **2017**, 29, 1605444; (e) R. Komatsu, H. Sasabe and J. Kido, *J. Photonics Energy*, **2018**, 8, 032108.

[2] (a) W. Song and J. Y. Lee, *Adv. Opt. Mater.*, **2017**, 5, 1600901; (b) K. H. Kim and J. J. Kim, *Adv. Mater.*, **2018**, 30, 1705600; (c) S. Scholz, D. Kondakov, B. Lüssem, and K. Leo, *Chem. Rev.,* **2015**, 115, 8449; (d) G. Li, Z. Q. Zhu, Q. Chen, J. Li, *Org. Electron.*, **2019**, 69, 135; (e) Y. Wang, J. H. Yun, L. Wang, and J. Y. Lee, *Adv. Funct. Mater.*, **2021**, 31, 2008332; (f) T. Chatterjee and K.T. Wong, *Adv. Optical Mater.*, **2019**, 7, 1800565; (g) H. Sasabe and J. Kido, *Chem. Mater.*, **2011**, 23, 621; (h) H. Sasabe and J. Kido, *J. Mater. Chem. C*, **2013**, 1, 1699.

[3] H. Fukagawa, T. Shimizu, H. Kawano, S. Yui, T. Shinnai, A. Iwai, K. Tsuchiya, and T. Yamamoto, *J. Phys. Chem. C,* **2016**, 120, 18748.

[4] (a) S. Schmidbauer, A. Hohenleutner, and B. König, *Adv. Mater.,* **2013**, 25, 2114; (b) F. So and D. Kondakov, *Adv. Mater.,* **2010**, 22, 3762; (c) S. Jhulki and J. N.

Moorthy, *J. Mater. Chem. C*, **2018**, 6, 8280.

[5] Y. Shirota and H. Kageyama, *Chem. Rev.*, **2007**, 107, 953.

[6] (a) H. Nakanotani, K. Masui, J. Nishide, T. Shibata and C. Adachi, *Sci. Rep.*, **2013**, 3, 2127; (b) L. S. Cui, S. B. Ruan, F. Bencheikh, R.Nagata, L. Zhang, K. Inada, H. Nakanotani, L. S. Liao and C. Adachi, *Nat. Commun.*, **2017**, 8, 2250; (c) T. Furukawa, H. Nakanotani, M. Inoue and C. Adachi, *Sci. Rep.*, **2015**, 5, 8429; (d) X. K. Liu, Z. Chen, C. J. Zheng, C. L. Liu, C. S. Lee, F. Li, X. M. Ou and X. H. Zhang, *Adv. Mater.*, **2015**, 27, 2378; (e) W. Liu, J. X. Chen, C. J. Zheng, K. Wang, D. Y. Chen, F. Li, Y. P. Dong, C. S. Lee, X. M. Ou and X. H. Zhang, *Adv. Funct. Mater.*, **2016**, 26, 2002.

[7] H. Uoyama, K. Goushi, K. Shizu, H. Nomura & C. Adachi, *Nature*, **2012**, 492, 234.

[8] (a) S. Watanabe and J. Kido, *Chem. Lett.*, **2007**, 36, 5; (b) T. Kamata, H. Sasabe, M. Igarashi, J. Kido, *Chem. Eur. J.*, **2018**, 24, 4590; (c) T. Kamata, H. Sasabe, N. Ito, Y. Sukegawa, A. Arai, T. Chiba, D. Yokoyama and J. Kido, *J. Mater. Chem. C*, **2020**, 8, 7200.

[9] (a) A. Lukyanov, C. Lennartz, and D. Andrienko, *Phys. Status Solidi A*, **2009**, 206, 12, 2737; (b) P. Friederich, F. Symalla, V. Meded, T. Neumann, and W. Wenzel, *J. Chem. Theory Comput.,* **2014**, 10, 3720; (c) N. B. Kotadiya, A. Mondal, S. Xiong,

P. W. M. Blom, D. Andrienko, and G.-J. A. H. Wetzelaer, *Adv. Electron. Mater.,* **2018**, 4, 1800366.

[10] (a) F. Suzuki, K. Shizu, H. Kawaguchi, S. Furukawa, T. Sato, K. Tanaka, and H. Kaji, *J. Mater. Chem. C*, **2015**, 3, 5549; (b) H. Uratani, S. Kubo, K. Shizu, F. Suzuki, T. Fukushima, and H. Kaji, *Sci. Rep.*, **2016**, 6, 39128; (c) S. Kubo, H. Kaji, *Sci. Rep.*, **2018**, 8, 13462.

[11] (a) N. Lin, J. Qiao, L. Duan, L. Wang, Y. Qiu, *J. Phys. Chem. C*, **2014**, 118, 7569; (b) M. Hong, M. K. Ravva, R. Winget, J. L. Brédas, *Chem. Mater.,* **2016**, 28, 5791.

[12] (a) D. F. O'Brien, P. E. Burrows, S. R. Forrest, B. E. Koene, D. E. Loy, M. E. Thompson, *Adv. Mater.,* **1998**, 10, 14; (b) P. M. Borsenberger, *J. Chem. Phys.*, **1991**, 94, 8276.

[13] H. Ishii, D. Tsunami, T. Suenaga, N. Sato, Y. Kimura and M. Niwano, J. Surf., *Sci. Soc. Jpn.*, **2007**, 28, 264.

[14] D. Yokoyama, *J. Mater. Chem.*, **2011**, 21, 19187.

[15] (a) H. Bässler, *Phys. Status Solidi B*, **1993**, 175, 15; (b) *Organic Photoreceptors for Imaging Systems*, ed. P. D. Borsenberger and D. S. Weiss, Marcel Dekker Inc., New York, **1993**.

[16] R. A. Marcus, N. Sutin, *Biochim. Biophys. Acta.*, **1985**, 811, 265.

[17] J. Kido, G. Harada, M. Komada, H. Shionoya and K. Nagai, *ACS. Symp. Ser.*, **1997**, 672, 381.

[18] P. Shrögel, N. Langer, C. Shildknecht, G. Wagenblast, C. Lennartz and P. Strohriegl, *Org. Electron.*, **2011**, 12, 2047.

[19] (a) Y. Nagai, H. Sasabe, J. Takahashi, N. Onuma, T. Ito, S. Ohisa and J. Kido, *J. Mater. Chem. C*, **2017**, 5, 527; (b) T. Ito, H. Sasabe, Y. Nagai, Y. Watanabe, N. Onuma and J. Kido, *Chem. Eur. J.*, **2019**, 25, 7308.

[20] (a) E. C. Riesgo, X. Jin and R. P. Thummel, *J. Org. Chem.*, **1996**, 61, 3017; (b) Y. J. Pu, G. Nakata, F. Satoh, H. Sasabe, D. Yokoyama and J. Kido, *Adv. Mater.*, **2012**, 24, 1765.

[21] Y. J. Pu, M. Miyamoto, K. I. Nakayama, T. Oyama, Y. Masaaki and J. Kido, *Org. Electron.*, **2009**, 10, 228.

[22] T. Matsushima, K. Goushi, C. Adachi, *Chem. Phys. Lett.*, **2007**, 435, 327.

[23] C. Féry, B. Racine, D. Vaufrey, H. Doyeux, S. Cinà, *App. Phys. Lett.*, **2005**, 87, 213502.

[24] H. Sasabe, S. Araki, S. Abe, N. Ito, K. Kumada, T. Noda, Y. Sukegawa, D. Yokoyama, J. Kido, *Chem. Eur. J.*, **2022**, e202104408.

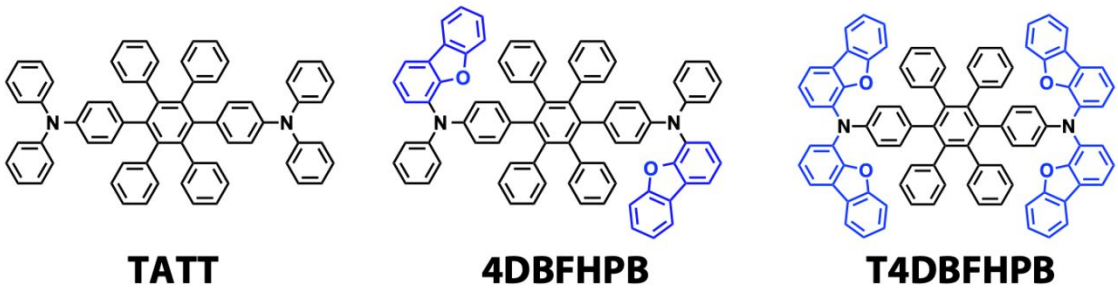

Figure 1. Chemical structures of the hole-transporters.

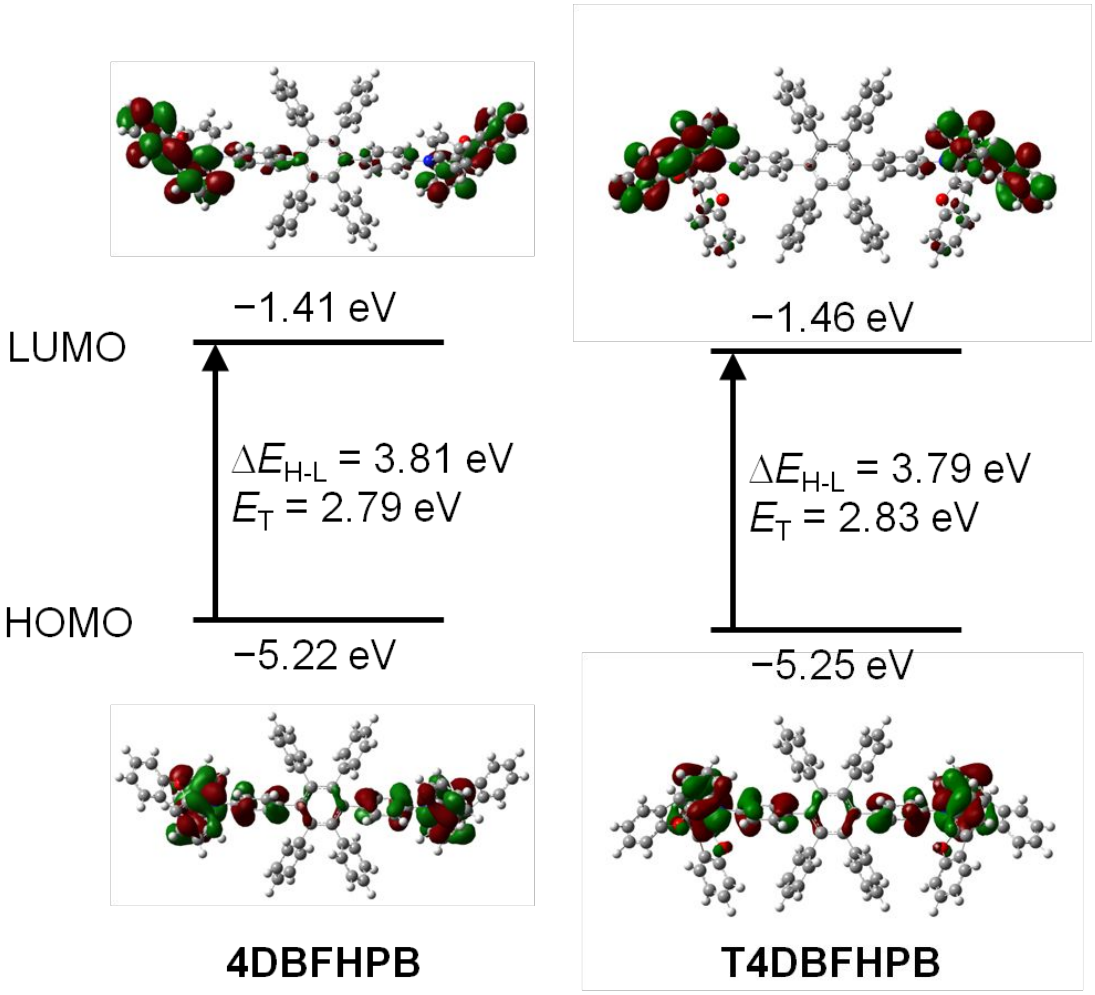

Figure 2. HOMO and LUMO distributions and energy levels, HOMO–LUMO energy differences (HOMO–LUMO), and the lowest triplet energy (E_T) for HTMs used in this study.

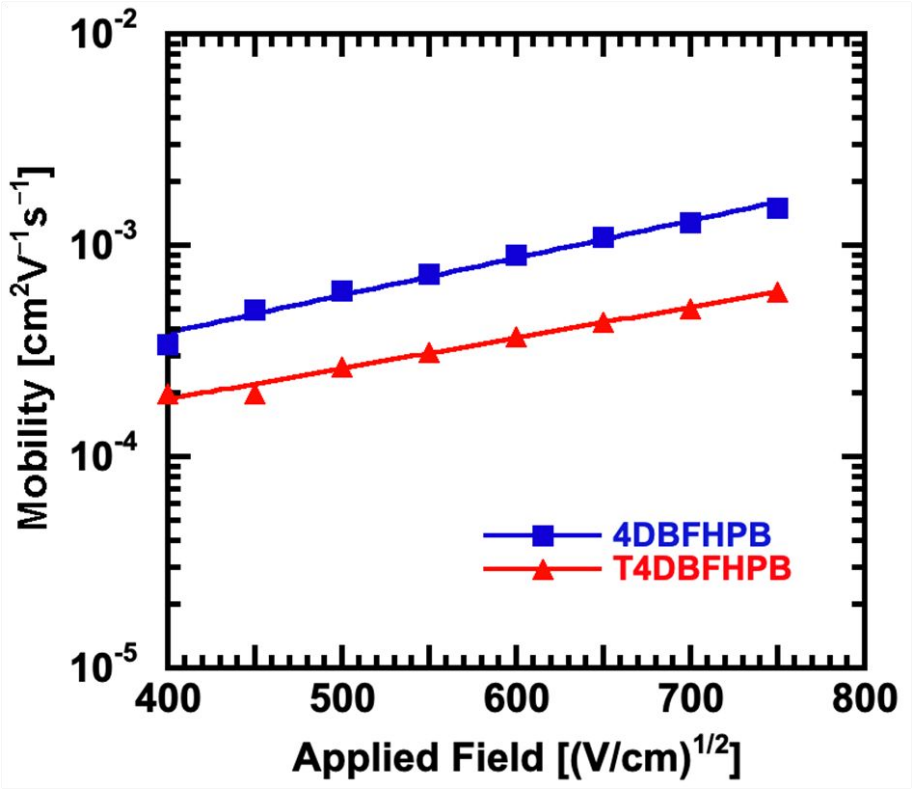

Figure 3. Experimentally-obtained hole-mobilities at 298 K plotted with respect to $F^{1/2}$ for HPB derivatives.

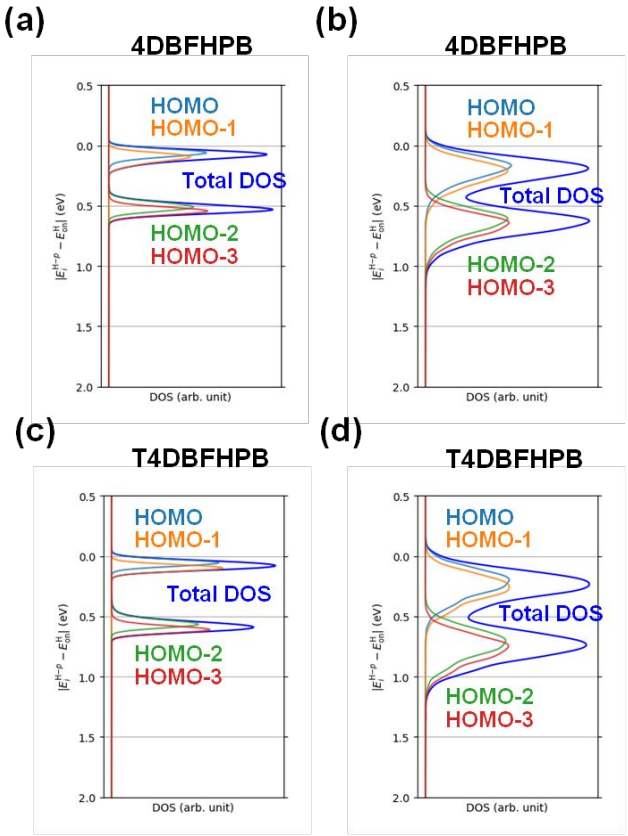

Figure 4. Density of states of **4DBFHPB** (a, b) and **T4DBFHPB** (c, d). a) and c) are distributions of eigenvalues without intermolecular interaction (intramolecular site energy), while b) and d) involve intermolecular interaction (intermolecular site energy). HOMO − p (p = 0, 1, 2, 3) were considered in the mobility calculations.

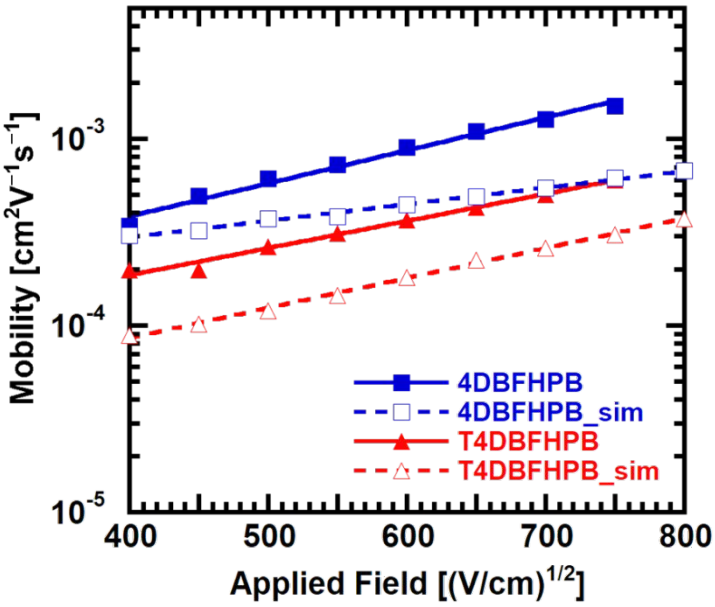

Figure 5. Simulated hole-mobilities for HPB derivatives and the TOF mobilities.

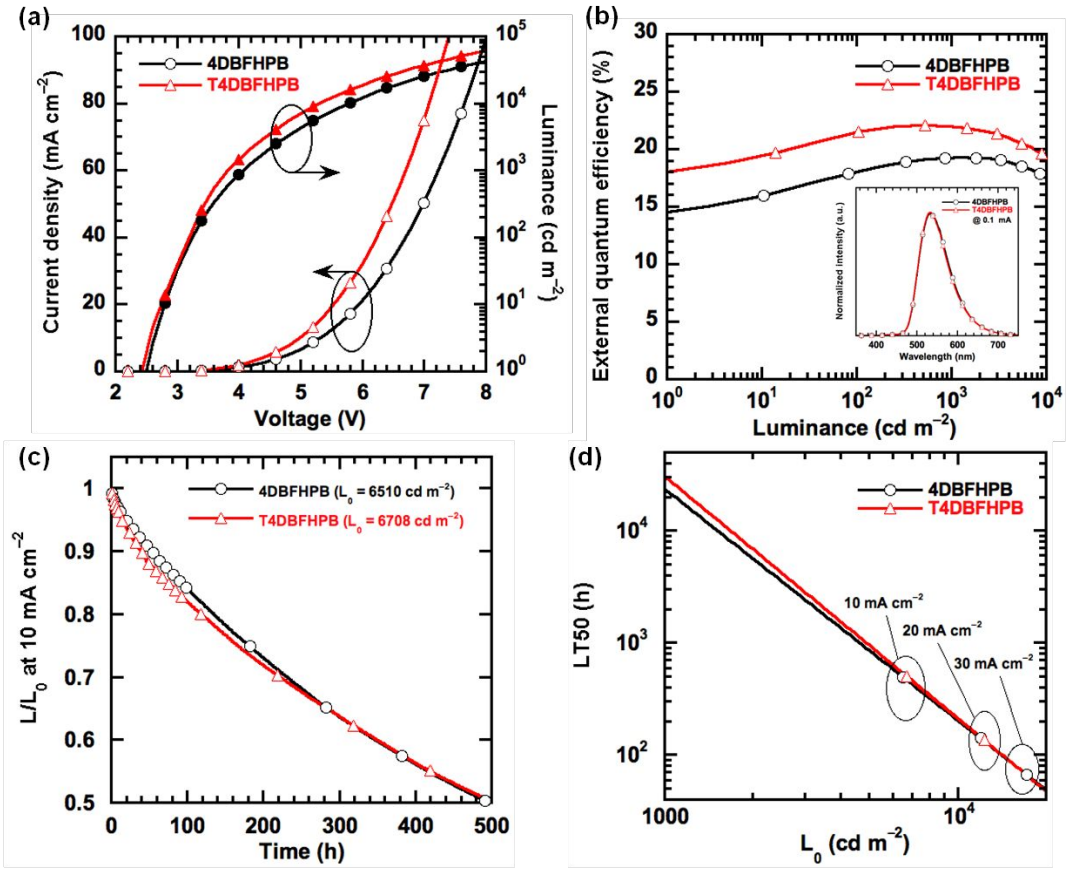

Figure 6. Device performance of green TADF OLEDs: a) *J*–*V*–*L* characteristics, b) η_{ext}–*L* characteristics (the inset shows EL spectra), c) operation lifetime at 10 mA cm^{-2}, and d) luminance acceleration tests of operation lifetime at 50% of the initial luminance.

Table 1. Thermal and optical properties.

Compound	Molecular weight	T_g[a]/T_m[a]/T_{d5}[b] (ºC)	HOMO[c]/LUMO[c]/E_T[d] (eV)	I_p[e]/E_g[f]/E_a[g]/E_T[h] (eV)
4DBFHPB	1049	135/313/490	−5.22/−1.41/2.79	−5.8/3.2/−2.6/2.7
T4DBFHPB	1229	171/364/494	−5.25/−1.46/2.83	−5.6/3.3/−2.3/2.8

[a]T_g and T_m were determined using differential scanning calorimetry. [b]T_{d5} was determined using thermogravimetric analysis. [c,d]Calculated at the RB3LYP 6-311+(d,p)/RB3LYP 6-31G(d) level. [d]Calculated triplet energy. [e]I_p was determined using photoelectron yield spectroscopy. [f]E_g was considered as the point at which the normalized absorption spectra intersected. [g]E_a was calculated with the use of I_p and E_g. [h]E_T was estimated from the onset of phosphorescent spectra at 5 K.

Table 2. Hole-transport parameters analyzed by using Gaussian disorder model.

Compound	μ_h[a] ($cm^2\ V^{-1}\ s^{-1}$)	μ_0[b] ($cm^2\ V^{-1}\ s^{-1}$)	σ[c] (meV)	Σ[d]	C[e] $(cm\ V)^{1/2}$
4DBFHPB	1.5×10^{-3}	1.67×10^{-2}	96	1.40	4.00×10^{-4}
T4DBFHPB	6.0×10^{-4}	1.13×10^{-2}	90	1.80	3.78×10^{-4}

[a]Hole-mobility at 5.6×10^5 V cm^{-1}. [b]Hypothetical mobility in a disorder-free system, [c]Energetic disorder, [d]Positional disorders, and [e]Empirical constants.

Table 3. Governing factors for the difference between hole-mobilities of **4DBFHPB** and **T4DBFHPB**.

Applied field $(V/cm)^{1/2}$	Electronic Coupling (%)	Intramolecular site energy (%)	Intermolecular site energy (%)	Reorganization Energy (%)
400	3.23	0.20	78.3	18.3
600	3.01	0.19	69.7	27.1
800	7.77	0.02	57.3	34.9

Table 4. Summary of OLED performances.

HTM	V_{on}[a] (V)	$V_{1000}/\eta_{c,1000}/\eta_{p,1000}/\eta_{ext,1000}$[b] (V/cd A^{-1}/lm W^{1}/%)	LT_{50} at 10 mA cm^{-2} (h)[c]	LT_{50} at 1000 cd m^{-2} (h)[d]	LT_{50} at 500 cd m^{-2} (h)[e]
4DBFHPB	2.45	4.07/66.7/51.5/19.2	497	~24,000	~100,000
T4DBFHPB	2.41	3.83/75.7/62.2/22.0	506	~28,000	~120,000

[a]Turn-on voltage at 1 cd m^{-2} [b]Voltage, current efficiency (η_c), power efficiency (η_p), and external quantum efficiency (η_{ext}) at 1000 cd m^{-2}. [c]Operation lifetime at 50% (LT_{50}) at a constant current density of 10 mA cm^{-2}. [d]LT_{50} of 1000 cd m^{-2} estimated by the luminance acceleration test. [e]LT_{50} of 500 cd m^{-2} estimated by the luminance acceleration test.

Table 5. Summary of reported OLED performances

	Emitter	V_{on}[a] (V)	$V_{1000}/\eta_{c,1000}/\eta_{p,1000}/\eta_{ext,1000}$[b] (V/cd A^{-1}/lm W^{-1}/%)	$\eta_{c,max}/\eta_{p,max}/\eta_{ext,max}$[c] (cd A^{-1}/lm W^{-1}/%)	LT_{50}[d] (h)	LT_{50}[e] (h)
This work	4CzIPN	2.41	3.19/73.8/72.8/21.4	72.7/71.3/21.4	860	28,000
Reference [6a]	4CzIPN	-	-/46.5/28.1/13.9	47.0/30.7/14.0	-	2800
Reference [6b]	4CzIPN	2.54	4.85/64.0/42.1/19.2	68.3/61.3/20.6	654	10,934
Reference [6c]	4CzIPN-Me	3.80	6.60/68.0/-/19.7	73.0/-/21.0	-	1472

[a]Turn-on voltage at 1 cd m^{-2} [b]Voltage, current efficiency (η_c), power efficiency (η_p), and external quantum efficiency (η_{ext}) at 1000 cd m^{-2}. [c]Maximum values of voltage, η_c, η_p, and η_{ext}. [d]Operation lifetime at 50% of the initial luminance of ~5000 cd m^{-2}. [e]Operation lifetime at 50% of the initial luminance of ~1000 cd m^{-2}.